frontiers | Frontiers in Earth Science

ORIGINAL RESEARCH
published: 27 May 2022
doi: 10.3389/feart.2022.884974

Mechanism of Coal Burst Triggered by Mining-Induced Fault Slip Under High-Stress Conditions: A Case Study

Jinzheng Bai[1,2]*, *Linming Dou*[1,2]*, *Jiazhuo Li*[1,3], *Kunyou Zhou*[1,2], *Jinrong Cao*[1,2] and *Jiliang Kan*[1,2]

[1]School of Mines, China University of Mining and Technology, Xuzhou, China, [2]State Key Laboratory of Coal Resources and Mine Safety, China University of Mining and Technology, China, [3]School of Mining Engineering, Anhui University of Science and Technology, Huainan, China

Coal burst disaster is easily triggered by mining-induced fault unloading instability involving underground engineering. The high-static stress environment caused by complex geological structures increases the difficulty in predicting and alleviating such geological disasters caused by humans. At present, the mechanism of coal burst induced by mining-induced slip fault under high-stress conditions still cannot be reasonably explained. In this study, the burst accidents occurring near mining-induced slip fault under high-stress conditions were carefully combined, and the "time–space–intensity" correlation of excavation, fault, and syncline and anticline structure of the mining areas was summarized. On this basis, the rotation characteristics of the main stress field of the fault surface subjected to mining under high-stress conditions and the evolution law of stress were analyzed. Last, based on the spectrum characteristics of mining-induced tremors, the first motion of the P-wave, and the ratio of Es/Ep, the source mechanism behind mining-induced fault slip under high-stress conditions was revealed. The results demonstrate that the coal burst triggered by the fault slip instability under high-stress conditions is closely related to the excavation disturbance and the fold structure. Mining activities trigger the unloading and activation of the discontinuous structural surface of the fault, the rotation of the stress field, and the release of a large amount of elastic strain energy and cause dynamic disasters such as coal bursts. The research results in this study are helpful to enrich the cognition of the inducing mechanism of fault coal burst.

Keywords: coal burst, mining-induced stress, fault slip, stress rotation, source mechanism

OPEN ACCESS

Edited by:
Kun Du,
Central South University, China

Reviewed by:
Guangan Zhu,
Xi'an University of Science and Technology, China
Zhenlei Li,
University of Science and Technology Beijing, China

***Correspondence:**
Jinzheng Bai
tb19020001b4@cumt.edu.cn
Linming Dou
lmdou@126.com

Specialty section:
This article was submitted to Geohazards and Georisks, a section of the journal Frontiers in Earth Science

Received: *27 February 2022*
Accepted: *11 April 2022*
Published: *27 May 2022*

Citation:
Bai J, Dou L, Li J, Zhou K, Cao J and Kan J (2022) Mechanism of Coal Burst Triggered by Mining-Induced Fault Slip Under High-Stress Conditions: A Case Study. Front. Earth Sci. 10:884974. doi: 10.3389/feart.2022.884974

INTRODUCTION

Coal burst can generally be classified into three types, i.e., the fault-induced type, the coal pillar-induced type, and the strain-induced type (Kaiser et al., 2000), in which fault-induced coal burst is caused by the superposition of the mining-induced quasi-static stress in the fault coal pillar and the seismic-based dynamic stress generated by fault activation (Cai et al., 2020). Coal burst triggered by mining-induced fault slip (CBTMIFS) refers to the dynamic phenomenon that the deep excavation activities lead to the fault's transformation from a locked state to an activated state, consequently resulting in sudden instability accompanied by violent energy release (Pan, 1999). Unlike natural earthquake induced by fault activation, mining activities are a key factor in the occurrence of

CBTMIFS (Ortlepp and Stacey, 1992). A strong mining tremor of magnitude 5.2 in 1997 is considered one of the largest seismic events recorded at the Klerksdorp mine in South Africa, and the analysis result of ground motion parameters indicates that the violent earthquake was attributed to an existing fault slip in the region (McGarr et al., 2002). In 2005, 112 shallow earthquakes were recorded during the construction of the MFS Faido tunnel in Switzerland, which were felt strongly on the ground and caused considerable damage to the tunnel. The focal mechanism solution was consistent with the strike and tendency of natural fault (Husen et al., 2013). On November 3, 2011, the F16 thrust fault was activated at the Qianqiu coal mine in Yima, Henan Province, China, causing 10 fatalities and trapping 75 miners. On March 27, 2014, another devastating burst accident of magnitude 1.9 in this coal mine caused 6 fatalities and trapped 13 miners. The accident investigation report pointed out that the key factor of the accident was slip activation of the thrust fault (Cai et al., 2018). The abovementioned dynamic disasters closely related to human mining activities have attracted extensive attention from the media and the public. If the internal mechanism of CBTMIFS can be revealed, important ideas can be provided for predicting and remitting the risk of such engineering disasters.

Different from the brittle shear deformation of faults, the fold structures such as syncline and anticline reflect the continuous ductile deformation of rocks under crustal movement and sedimentation (Suppe, 1983). Both faults and folds are widely distributed in nature, often in the same tectonic unit. For large-scale crustal movements, multiple fold and fault structures interact and mutually transform through interlayer slip, uplift, and fold during the long historical tectonic movement and sedimentation process, and the specific forms include fault-related fold, fault-transition fold, fault-propagation fold, fault-detachment fold, imbricate structure, wedge structure, and interference structure(Bieniawaki, 1967). For the medium- and small-scale production range of mining areas, the frequent geological movement dominated by ancient stress leads to the complex regional tectonic stress field. Therefore, it will be more difficult to investigate the disaster-triggering mechanism of the mining-induced fault slip under a high-stress engineering background.

In order to clarify the occurrence mechanism of CBTMIFS in geological anomaly areas, plenty of studies have been carried out through theoretical analysis, laboratory experiment, numerical simulation, and field experiment,including the mechanical response and mineral composition of fault gouge (Morrow and Byerlee, 1989), hydraulic pressure and stress state of the fault zone (Segall and Rice, 1995), slip and failure criterion of fault (Fan and Wong, 2013), and energy accumulation and release law of the fault surface (Zhao and Song, 2013). On this basis, the key scientific issues condensed include the following: *1*) How engineering dynamic disturbances, such as blasting, TBM excavation, hydraulic fracturing, geological drilling and rockburst, natural earthquake, driving load, and continuous explosion, will lead to slip, failure, and even instability of faults in high-stress geological anomaly areas? *2*) What response characteristics will be caused to the stress field, vibratory field, and energy field of surrounding rock in the adjacent production area once the fault instability occurs in the high-stress geological anomaly area?

Relevant studies suggest that local high-stress concentration is likely to occur and develop when the mining working face or the excavation boundary is close to the fault in the high-stress geological anomaly area, and the corresponding burst risk increases (Cook, 1976; Blake and Hedley, 2003; Yin et al., 2014). When the fault approaches the critical stress state, the normal stress and the shear stress decrease sharply due to the reduction of intergranular force and the contact fracture of particles, and the evolution of fault state depends on the initial stress condition and excavation process (Wu et al., 2017; Yin et al., 2012). Field observations and theoretical analysis show that the development height of mining-induced fault rupture and slip is controlled by the magnitude and direction of principal stress, while the intensity of seismic events is related to the stratum matrix and local fractures involved in the rupture process (Duan et al., 2019). At the same time, many investigations have explored the response behavior of faults to static and dynamic load disturbances by changing stress conditions in laboratory tests. Marone (1998) pointed out that static friction and aging strengthening of faults are systematic responses that depend on loading rate and elastic coupling. Li et al. (2011) simplified the normal behavior of faults to elastic stiffness, adopted the coulomb-slip model to characterize the shear behavior of faults, and conducted a quantitative study on the propagation and attenuation law of seismic waves in discontinuous rock masses. Bai et al. (2021) introduced the displacement-related moment tensor method to reproduce the phenomenon of mining-induced fault slip of coal mine site in numerical simulation.

To sum up, the stress distribution and evolution characteristics of conventional fault activation instability have been well researched on. However, there are few studies on CBTMIFS under high-stress environments, and the existing research results ignore the influence of mining quasi-static loading and unloading stress paths and ground motion stress on the fault slip instability. Therefore, it is necessary to further study the mechanism of CBTMIFS under high-stress conditions, for providing guidance for the monitoring and prevention of coal bursts induced by fault instability.

SITE DESCRIPTIONS

Geological Structures

Mengcun coal mine mainly mines 4# coal seam, where is located in Binchang coal district, Shaanxi province, China, with a mining depth of 620–750 m. The 401101 working face is the first working face of the Mengcun coal mine, with a length of 2090 m and a width of 180 m. The layered fully-mechanized sub-level caving mining technology is adopted. *See* **Figure 1**, the north wing, west wing, and east wing of the working face are solid coal, and there is a 200 m protective coal pillar between it and the main entry group. The development roadway includes five main entries, which are no.2 return air main entry, no.2 belt main entry, band conveyer main entry, no.1 belt main entry, and no.1

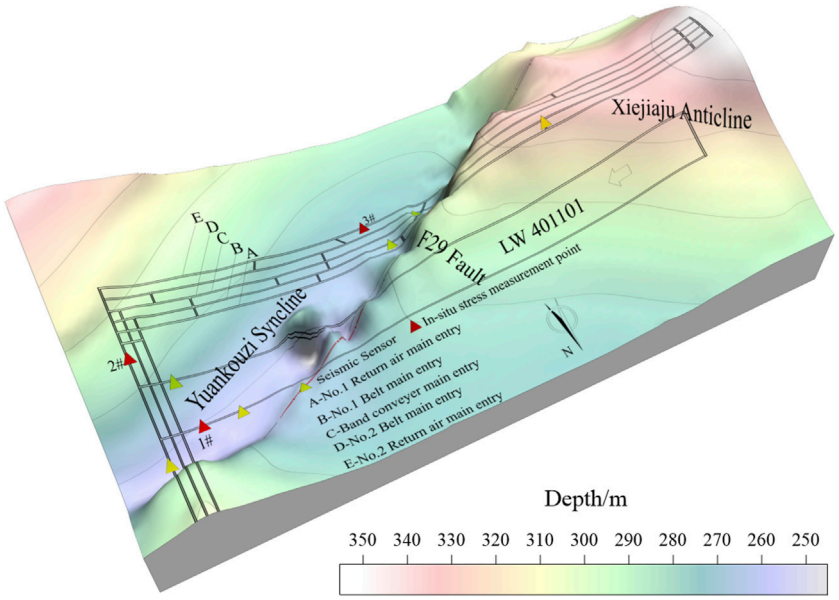

FIGURE 1 | 3D view of a mine's working face, geological structure, ground stress and microseismic measurement point.

TABLE 1 | Major geological tectonic parameters of the minefield.

Tectonic name	Occurrence		
	Dip angle (°)	Inclination angle (°)	Drop (m)
F29 normal fault	150	60–70	15–18
Yuankouzi syncline (X1)	Axial direction: NE; extending length: 1455 m; dip angle of coal seam: 5–8°		
Xiejiazui anticline (B2)	Axial direction: NEE; extending length: 2286 m; dip angle of coal seam: 3–8°		

return air main entry from north to south, with a width of coal pillars between the entries of 35 m. The average thickness of 4# coal is 20 m, and the average dip angle of the coal seam is 4°. The roof is mainly made of sandy mudstone, fine-grained sandstone, and coarse-grained sandstone, and the bottom plate is mainly made of aluminum mudstone which tends to expand when meeting water. After identification, 4# coal seam has strong burst liability, the roof has weak burst liability, while the floor has no burst liability.

Tectonic Parameters

Xiejiazui anticline (B2), Yuankouzi syncline (X1), and F29 normal fault occur from west to east in the minefield area. The faults' location between the syncline and anticline structures forms a special geological structure group, thus mainly controlling the gestation, evolution, and occurrence process of coal burst accidents in this region. Detailed geological and tectonic parameters are displayed in **Table 1**.

To further explore the influence degree of geological structure on the distribution of ground stress field in the mining area, three ground stress measurement points were arranged in the areas of central main entries, panel main entries, and the 401101 working face. Meanwhile, the ground stress of hollow inclusion was measured. As shown in **Figure 2**, the vertical stress in this area is the minimum principal stress, the results of three measurement points are basically consistent with the average stress level of the Binchang coal district and the Chinese mainland. Due to the presence of faults and fold structures, horizontal tectonic stress is the main stress component in the regional high-stress environment. The results of the three measurement points are obviously higher than the average stress levels of both the Binchang coal district and the Chinese mainland, especially the measurement point 3# is closer to the X1 axis and F29 fault, where σ_H/σ_V reaches 2.1. The results indicate that the closer it is to the fault and synclinal axis, the more abnormal its horizontal stress is.

As shown in **Figure 3**, four geological exploration boreholes, M2-1, M3-2, M4-2, and M5-2, were selected in the main entries and the 401101 working face to analyze the influence of the composite geological tectonic group on regional stratigraphic sediment characteristics. It can be concluded that: *1*) The regional strata are mainly composed of alternately deposited fine-grained sandstone, medium-grained sandstone, coarse-grained sandstone, and sandy mudstone, and no thick whole layer of hard sand-gravel rock exists. *2*) In the long process of

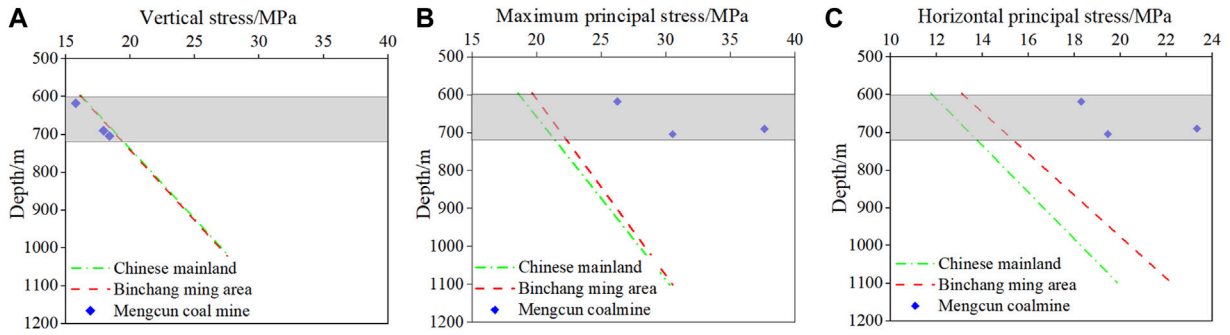

FIGURE 2 | Comparison diagram of ground stress results and *in-situ* stress values in Binchang mining area and Chinese mainland. **(A)** Vertical stress; **(B)** Max principal stress; **(C)** Horizontal principal stress.

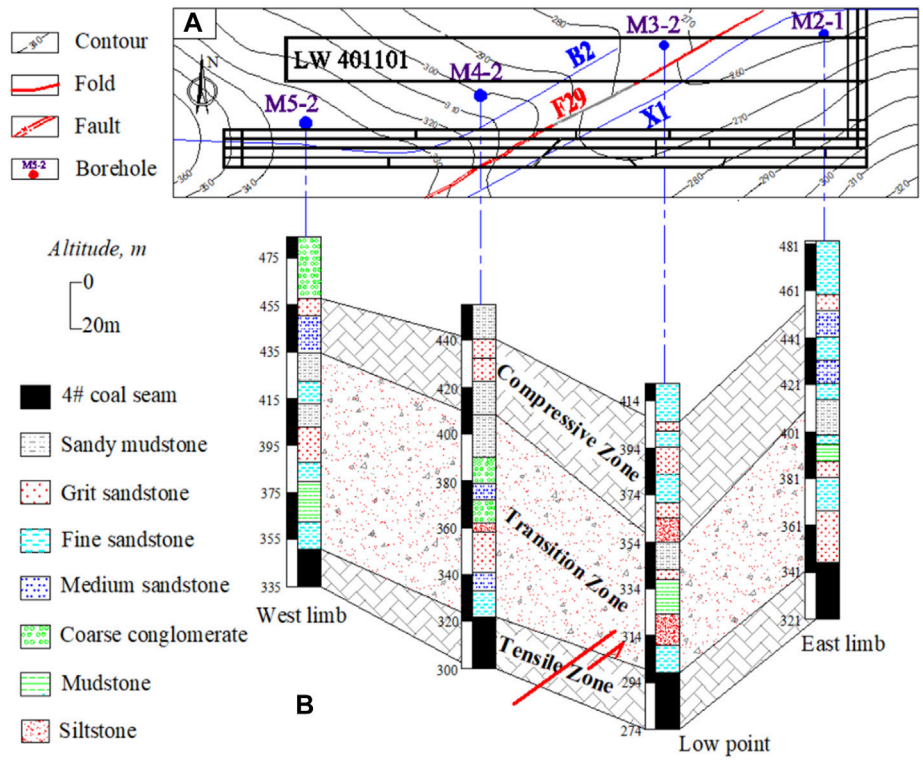

FIGURE 3 | Stratigraphic map of the coupled fault-fold region near the 401101 working face. **(A)** Geological exploration boreholes of LW 401101; **(B)** Regional stratigraphic sediment characteristics.

crustal movement and evolution, stratum inversion and deletion occur frequently among the upper overburden strata. Affected by the extrusion tectonic stress in the east and west direction, faults and relative slips occur in weak coal seams, which are upright or inverted and thus form compression-torsion faults. The strata are obviously controlled by the tectonic movement of faults and folds. *3*) Relatively, the difficulty of mining increases as the strata near the M4-2 borehole is not only squeezed by horizontal tectonic stress of fold, but also affected by vertical dislocation of the F29 normal fault, which results in the discontinuity of the strata, with stress concentration and energy accumulation. Therefore, unstable stratum deposition and phase transition provide a favorable external environment for frequent coal burst accidents in this region.

COAL BURST HISTORY

The inducing process of coal burst is very complex, which is not only affected by geological structures such as folds and faults but

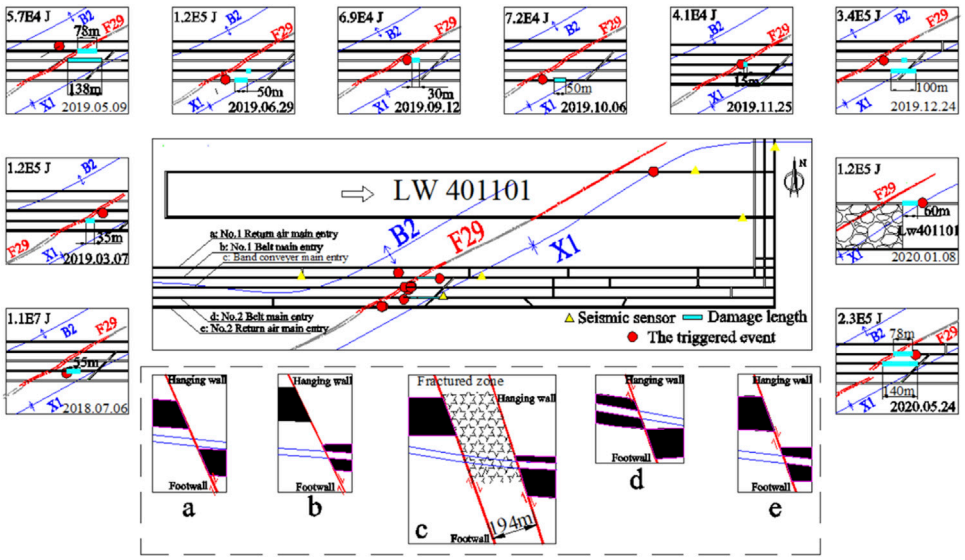

FIGURE 4 | Map of the locations of the previous bursts and the faults of each main entries.

also closely related to the mining activities involved (Zhang et al., 2017; Yin et al., 2019). Therefore, it is of great significance to clarify the relationship between coal bursts and geological structure and mining activities in this region. The mining of the 401101 working face started in June 2018 and ended in March 2020, during which a total of 10 coal burst accidents occurred. The SOS microseismic system was arranged in working face and main entries, which could monitor the vibratory signal in the mining process. The distance between the seismic source and the fault and the on-site failure range monitored when the burst occurred are presented in **Figure 4**, and the on-site burst failure is in **Figure 5**.

Figure 4 demonstrates that all previous coal burst accidents have significant common characteristics: *1*) Most of the coal bursts occurred in the main entry area, which is obviously inconsistent with the distribution law of mining-induced tremors commonly seen near the mining working face. *2*) Most of the coal bursts occurred on the hanging wall of the F19 fault, while there are relatively few occurred on the footwall of the F19 fault, showing an obvious hanging wall effect. This is in agreement with the existing research conclusions: in the field of seismology, the hanging wall's ground motion is stronger than the footwall, its vibration attenuation is weaker than the footwall, and its vibration distribution area is larger than the footwall in natural fault shear slip. *3*) The minimum destructive microseismic energy detected during a coal burst is 2.6 E+04 J, and the corresponding failure range of the entry is only 3 m; the maximum microseismic energy is 3.5 E+05 J, and the corresponding failure range of the entry is 55 m, showing that the more elastic energy released during a coal burst, the greater the influence on entry stability. *4*) The burst frequency and range of the five main entries are not completely consistent, the situation of <C> band conveyer main entry and <D> no.1 belt main entry is the most dramatic, showing the overall characteristics of multiple and repeated bursts. As shown in **Figures 4A–E**, considering different actual exposure of each entry of the F29 fault surface, especially when the band conveyer main entry passes through the fault, there is an obvious fracture zone between the hanging wall and the heading wall with a thickness of about 194 m, which has a negative effect on the stability of surrounding rock of the entry, it is speculated that the heterogeneity of coal burst frequency and intensity of each main entry is related to the heterogeneous evolution of shear stress along the F29 fault surface. *5*) The occurrence of coal bursts is significantly affected by mining disturbance. Only one coal burst accident occurs after the stoppage of mining activities, suggesting that the frequent occurrence of coal bursts on the fault surface is closely related to mining activities. *6*) The occurrence of coal burst is affected by B2 anticline to a certain extent, but it is affected by F29 fault and X1 syncline significantly. Especially in the composite area of F29 fault and X1 syncline, coal burst accidents occur intensively.

Figure 5 shows the entry damage caused by the coal burst. The overall damage characteristics can be divided into four categories: floor bulge, roof caving, support failure, and equipment damage. Floor damage can be divided into raising, side lifting, overall drum, and cracking; equipment damage can be divided into belt tilting, tub overturning, platform overturning, and pipeline falling; support failure can be divided into anchor slipping, cable overhanging, bolt shearing, and tray rushing out; roof caving can be divided into step sinking, drossy coal falling, roof separation, and roof falling. Different from conventional coal bursts, this kind of coal burst has significant shear seismic failure characteristics, with a more complex failure type, a larger failure range, and a higher failure degree.

Therefore, it is preliminarily inferred that the controlling factors of frequent coal burst accidents in the main entry area are as follows: influenced by bedding or lateral compression of

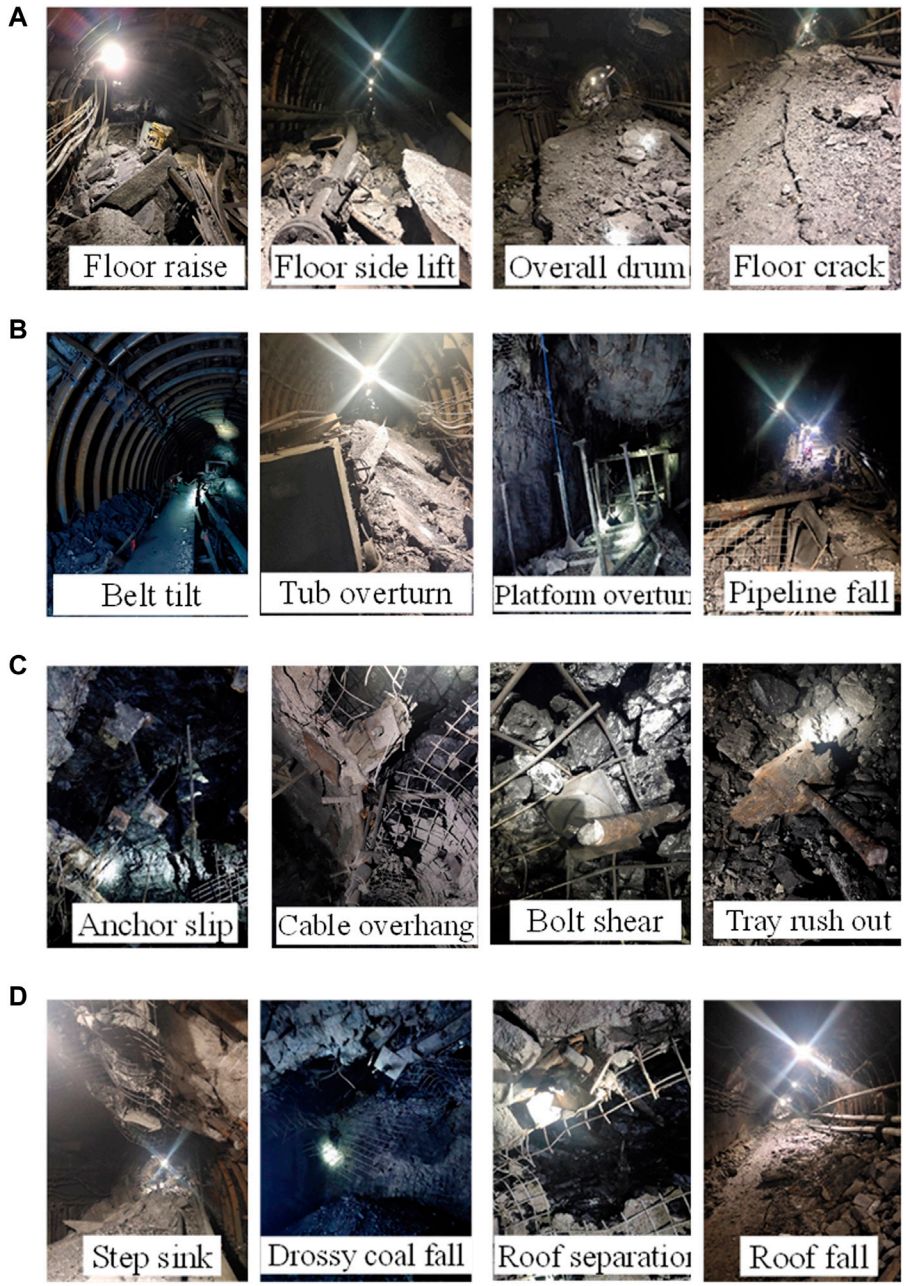

FIGURE 5 | Pictures of burst failure of coal burst on site. **(A)** Floor bulge; **(B)** Equipment damage; **(C)** Support failure; **(D)** Roof caving.

regional strata, the compound tectonic condition of B1 anticline and X1 syncline provides a high-static-stress environment for the main entry area. The F29 fault with a drop of 15–18 m crosses diagonally both main entries and the 401101 working face. Under the tectonic influence, a large amount of elastic energy is accumulated of the fault surface, which lays an energy foundation for the occurrence of coal bursts. Human activities, including excavation, mining, and entry expansion, lead to different stress adjustment ranges and intensities and result in different degrees of damage in main entries. To further verify the rationality of the hypothesis, the stress evolution law on the fault during the mining process was analyzed by numerical simulation.

STRESS FIELD MODELING OF INTERFACE IN F29

Model Setup and Constrains

FLAC^{3D} (Fast Lagrangian Analysis of Continua in 3 Dimensions) was employed to analyze the stress distribution of the fault surface

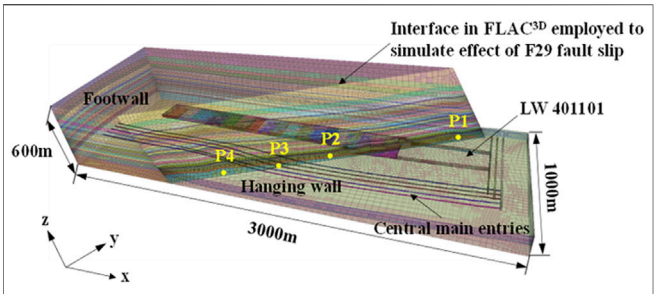

FIGURE 6 | Sketch map of initial numerical simulation and measurement points.

of F29 and in the coal pillar around the main entries of the 401101 working face during the whole stopping period. The geometric dimension of the model is 3,000 × 1,000 × 600 m. Normal displacements are fixed at the base and the sidewalls of the model. In view of the complex layout condition that five main entries cross the F29 fault as well as coal rock seam, high-precision modeling shown in **Figure 6** was realized by Rhino software, in which X1 syncline and B1 anticline generated 3D undulated strata through real coal floor contour lines for restoration. F29 fault was generated according to actual fault parameters with a fault surface dip angle of 75° and a height difference of 20 m. The strain-softening criterion was adopted to judge the yield state of materials and determine the physical mechanics parameters of both coal rock mass and fault slip surface. The parameters are listed in **Tables 2**, **3**, respectively. As displayed in **Figure 6**, four monitoring points were successively arranged along the F29 fault surface in the model.

The steps of numerical simulation are as follows:

1) According to the real ground stress test results, 30 MPa horizontal stress and 20 MPa vertical stress were applied to the model to balance the initial ground stress field and complete the excavation of the development roadway and main entries.
2) The 401101 working face was excavated step by step. The stress distribution in the coal pillar near the main entries, and the normal stress and shear stress distribution of the F29 fault surface were monitored.
3) Taking σ_h = 30 MPa, σ_v = 20 MPa, and the lateral pressure coefficient b = 1.5 as initial values, the effects of different horizontal ground stress on normal stress and shear stress of the fault surface in the mining process were analyzed when b equals 0.5, 1, 1.5, 2, and 2.5, respectively.

Influence of Mining Activities on the Stress Distribution of the Fault Surface

Figure 7 presents the changes in stress evolution of the fault surface at P1, P2, P3, and P4 when the lateral pressure coefficient b is 0.5. The stress at each monitoring point evolves dynamically with the advance of the working face. The change laws of normal stress and shear stress between the monitoring points are different, indicating that the stress of the fault surface is not evenly distributed due to mining disturbance, which leads to the regional difference in burst risk.

As illustrated in **Figure 7A**, due to mining disturbance, the normal stress and shear stress of the fault surface at P1 on the north side of the working face almost synchronously fluctuate sharply, in which the normal stress drops rapidly first and then recovers to a certain level with a fluctuation value of about 1.2 MPa; the shear stress first increases slightly and then decreases rapidly to a certain level, with a fluctuation value of about 3.0 MPa. As shown in **Figure 7B**, when the working face continues to advance, both the normal stress and shear stress at P2 on the south side of the working face show an upward trend, with a fluctuation value of shear stress of about 3.0 MPa, while that of normal stress of about 0.4 MPa. It suggests that the remote mining activities still have slight disturbance to the fault surface in a metastable state, which

TABLE 2 | Physical mechanics parameters of coal rock seam.

Rock property	Density/ g·cm^{-3}	Bulk modulus/ GPa	Shear modulus/ GPa	Tensile strength/ MPa	Cohesive force/ MPa	Friction angle/°	Residual cohesive forces/ MPa	Residual internal friction angle/°
Mudstone	2200	1.67	0.77	2.5	3.0	20	0.4	10
4# coal coal	1340	2.0	0.8	2.2	3.0	28	1.0	20
Coarse sandstone	2300	3.53	2.81	4.5	6.0	26	2.5	15
Medium-grained sandstone	2520	3.45	3.15	9.0	14.0	30	—	20
Fine-grained sandstone	2520	4.90	3.60	12.0	16.0	35	5.0	25
Siltstone	2520	3.2	2.8	6.3	8.67	29	4.0	20

TABLE 3 | Physical mechanics parameters of the fault interface.

Normal stiffness /GPa·m^{-1}	Shear stiffness /GPa·m^{-1}	Internal friction angle /°	Cohesive force /MPa
1.0	1.0	30	0.1

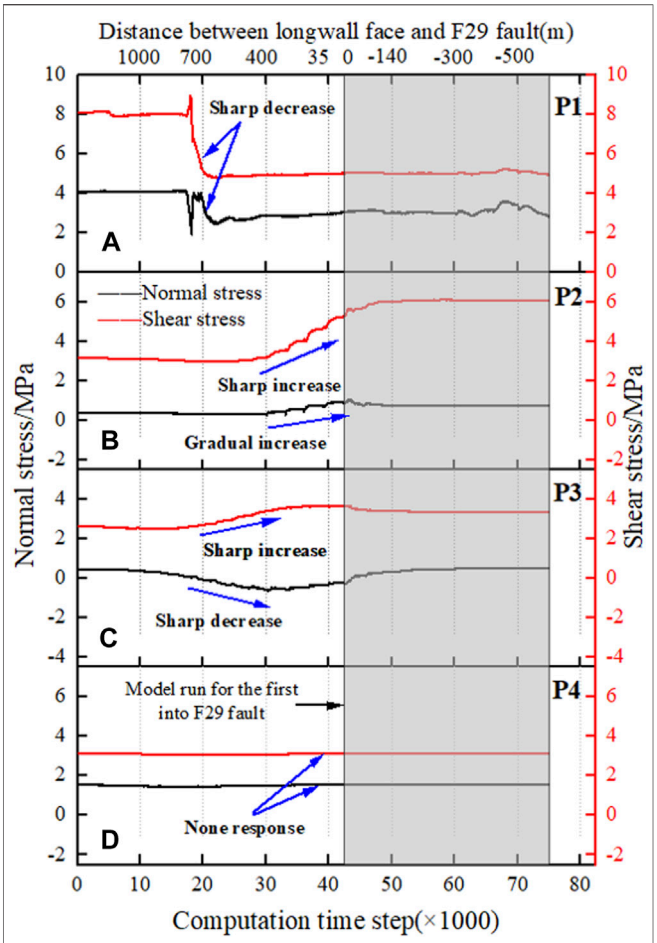

FIGURE 7 | Change laws of normal stress and shear stress with working face advance. **(A)** P1; **(B)** P2; **(C)** P3; **(D)** P4.

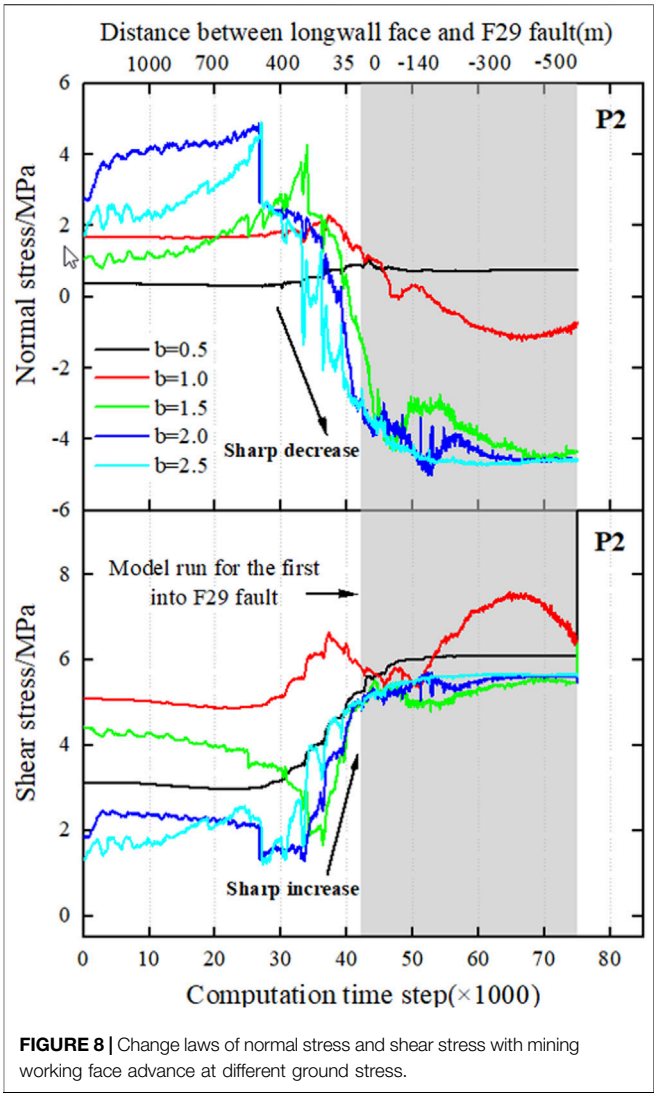

FIGURE 8 | Change laws of normal stress and shear stress with mining working face advance at different ground stress.

results in the instability of the fault with a quantity of originally accumulated strain energy, thus releasing strain energy outward, and this process is likely to induce coal burst accidents.

As illustrated in **Figure 7C**, when P3, located between no.2 return air main entry and no.2 Belt main entry, is 700 m away from the fault of the working face, the normal stress plunges, while the shear stress increases sharply. It is worth noting that the value of normal stress experiences a "positive-negative-positive" change process, suggesting that the main stress field of the fault surface rotates due to mining disturbance, which can be considered as a precursor of fault slip. As displayed in **Figure 7D**, due to the long distance between the working face and P4 located in the south of no.1 return air main entry, basically no stress response is generated during the whole mining process of the working face and the burst risk is relatively low, which is consistent with the situation that only one burst accident occurred in no.1 return air main entry.

Influence of Ground Stress on the Stress Distribution of the Fault Surface

To further investigate the inducing law of high stress caused by the fold structure to mining-induced slip fault, **Figure 8** shows the change laws of normal stress and shear stress at P2 located between the 401101 working face and the main entry group with mining advancement under different ground stress conditions (that is, when the lateral pressure coefficient b is 0.5, 1.0, 1.5, 2.0, and 2.5, respectively). As can be seen from **Figure 8**, the evolution laws of normal stress and shear stress at this measurement point are basically consistent at different ground stress levels.

When the horizontal stress is low while *b* is 0.5 and 1.0, the working face advances to about 400 m of the fault, the normal stress rises slightly, and the shear stress rises more sharply than the normal stress. When horizontal stress further rises, while *b* is 2.0 and 2.5 m, the normal stress of F29 fault shows a drastic downward trend, on the contrary, the shear stress dramatically increases, and the response time is advanced, showing that a high-stress environment provides a good condition for strain energy accumulation of the fault, which leads to a significant expansion of the range affected by mining activities. When the horizontal stress is higher, the value of the normal stress changes more from "positive value to a negative value and then to a positive value,"

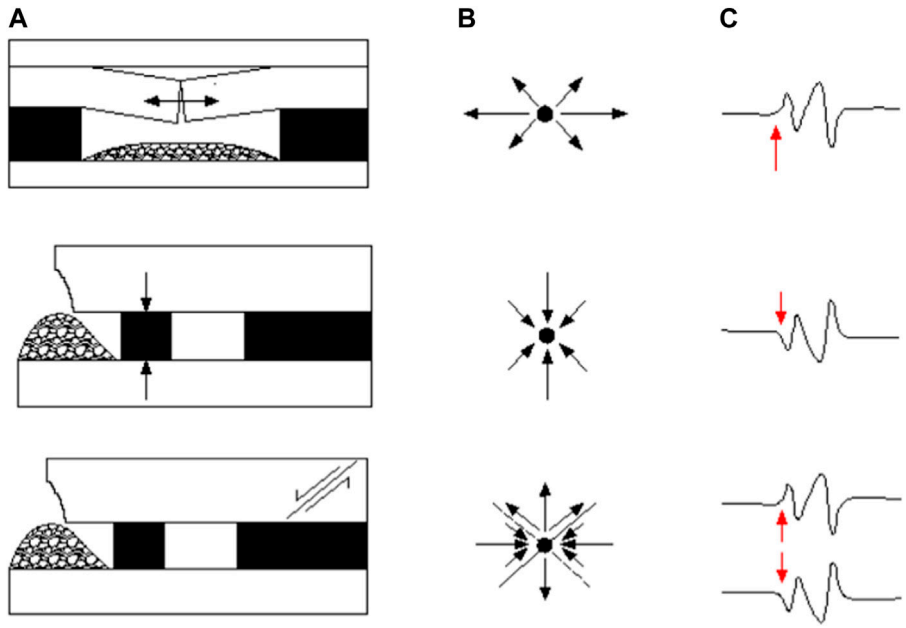

FIGURE 9 | Typical tremor model. **(A)** Types of mining-induced tremors; **(B)** Patterns of P-wave radiation; **(C)** Directions of P-wave first motion.

with higher intensity of energy accumulation and release, higher corresponding burst risk, and thus more likeliness of coal bursts. This conclusion reflects the mechanism of the fold structure on mining-induced fault slip.

MECHANISM OF COAL BURST REVEALED BY MS EVENTS

The focal rupture mechanism of coal rock spontaneous mining-induced tremors resembles that of natural earthquakes. In the past, people mainly used the occurrence mechanism of natural earthquakes to reveal the seismic source rupture process of most mining-induced tremors (McGarr, 1984; Gibowicz and Kijko, 1994). However, the geological structure, excavation environment, and overburden structure of a mine determine the particularity and complexity of the seismic source of a mining-induced tremor. Different causes of mining-induced tremors and different focal rupture mechanisms lead to the disparity in the energy release size of mining-induced tremors and in radiation modes of shake displacement wave field. As displayed in **Figure 9**, according to the seismic source acting force modes of mining-induced tremors and the relative position relationship between the coal rock failure area and the working face, mining-induced tremors can be simply divided into three types: tension type, implosion type, and shear type (Horner and Hasegawa, 1978; Hasegawa et al., 1989). The tension type and the implosion type are dominant, while the shear-type caused by a dynamic slip of fault is infrequent. At the same time, the waveform of mining-induced tremors contains abundant focal rupture mechanisms, and the application of seismology in the field of coal rock-burst rupture is beneficial for promoting the study of the focal rupture mechanism of mining-induced tremors. This section attempts to discuss the focal rupture mechanism of frequent coal bursts in the main entries from the aspects of spectrum characteristics of shake displacement, P-wave first motion, and the ratio of E_S/E_P.

Waveform and Frequency-Spectra Characteristics of Mining-Induced Tremors

The typical clear waveform monitored by the microseismic station of three typical tremor events "2019.09.12," "2020.01.08," and "2020.05.24" were selected to determine the main frequency segment by frequency-spectra analysis. In the process of propagation, the tremor wave carries important information that can reflect the characteristics of the stratum and the source, such as fault, fractured zone, geological acoustics characteristics, and focal mechanism characteristics, which are mainly reflected in the attenuation of seismic wave intensity, frequency structure characteristics, and local singularity of signal. In so many computing methods of fractal dimension, the box dimension index Dq is employed in this study to define the burst waveform.

Taking $N(\Delta)$ as the minimum number of a square box with a side length of Δ covering a point set, then the box dimension of the point set is defined as

$$D_q = -\lim_{\Delta \to 0} \frac{\lg N(\Delta)}{\lg \Delta}. \quad (1)$$

As shown in **Figure 10**, the spectrum of each burst event is noisy and sharp, the signal is complex, and there is a great difference between each channel, which indicates that the

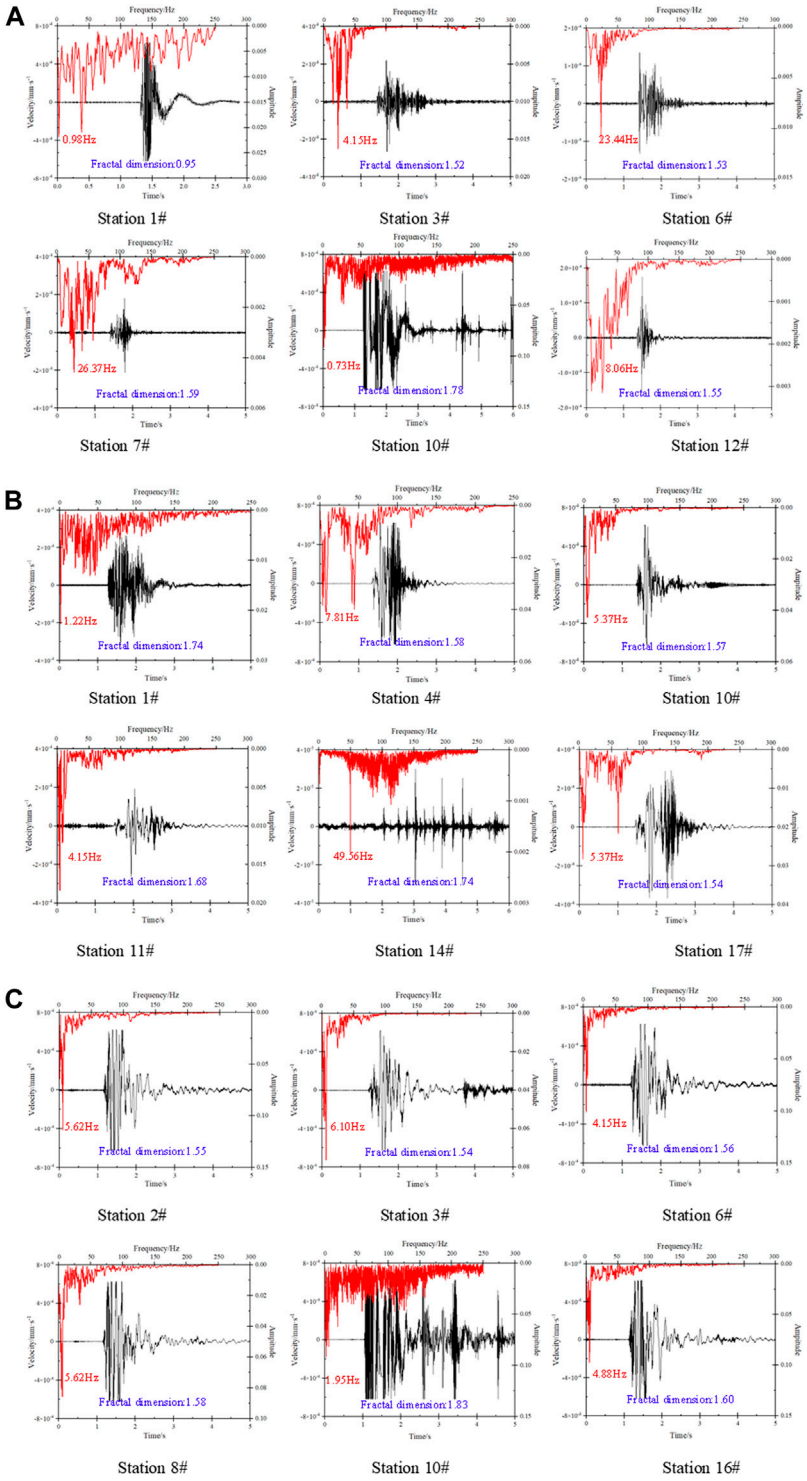

FIGURE 10 | Typical burst waveform, frequency spectrum characteristics and fractal dimension. **(A)** The "2019.09.12" burst event; **(B)** The "2020.01.08" burst event; **(C)** The "2020.05.24" burst event.

discontinuity surface of the F29 fault and the goal of the 401101 working face change the propagation characteristics of the seismic wave. Overall, the duration of typical seismic signals is about 2,500–3,500 ms, and the seismic velocity is about 2.0×10^{-4}–6.0×10^{-4} mm/s. The frequency is mainly distributed between 0–30 Hz with the main frequency mostly

lower than 10 Hz, and the middle and high-frequency components attenuate notably, reflecting a characteristic of "high energy and low-frequency" of mining-induced tremor waveform. The fractal dimension *D* of each channel ranges from 0.95 to 1.78, which fully indicates the disorder and complexity of these burst tremors. Different from small and medium energy mining-induced tremors, the burst mining-induced tremor has a more rapid process from fracturing to receiving signal, its amplitude of P-wave first motion is weak and even difficult to identify. Furthermore, its energy release and dissipation are more violent. Another evident feature is that the shear rupture waveform reflecting the tangential deformation of coal rock units is relatively developed, and the amplitude of S-wave first motion is obvious, which accords with the common shear seismic waveform characteristics (Du et al., 2021).

Taking stations 1# and 10# in the "2019.09.12" burst event, stations 1# and 17# in the "2020.01.08" burst event, and stations 6# and 8# in the "2020.05.24" burst event as examples, the following phenomena can be observed. The coda waves of mining-induced tremor waveform monitored by them are relatively developed; the spectrum development shows a violent oscillation characteristic; the middle part of the waveform presents a shape of "inverted triangle graben"; and the whole waveform exhibits a nonlinear and multi-period disturbance characteristic. This corresponds to the ultra-low friction effect of faults and the dynamic activation instability of faults under the effect of dynamic load, which is consistent with the propagation characteristics of ultra-low-frequency, low speed, and high energy of over range pendulum-shaped waves under the effect of discontinuous and uncoordinated deformation of faults.

In addition, the waveforms monitored by station 10# in the "2019.09.12" burst event, station 14# in the "2020.01.08" burst event, and station 10# in the "2020.05.24" burst event still have secondary vibrations and even frequent vibrations after the end of the mainshock. The phenomenon of "main shock-after shock" reflects that these burst events have waveform characteristics like earthquakes induced by fault slip.

P-Wave First Motion of Mining-Induced Tremors

Byerly (1928) was the first to use the four-quadrant distribution of the compression and expansion of P-wave first motion to explore the nature of the seismic source, and he believed that the direction of P-wave first motion on the vibration sociogram was directly related to the seismic source force. As the physical image of the waveform was clear and not affected by the crustal velocity structure, it can be employed to preliminarily determine the focal mechanism solution (Herrmann, 1975). The coal rock mass fracture, such as horizontal tension fracture of the roof, longitudinal separation, and roof caving, generates the compression P-wave leaving the seismic source and the front part pushing outward. The P-wave first motion received by the microseismic station is "+," and this kind of tremor belongs to a typical tension type. The vibration, such as roof rotation instability and coal pillar compression fracture, generates the expansion P-wave pointing to the seismic source and its front part pulling outward. The P-wave first motion received by the microseismic stations is "–," and this kind of coal rock-induced tremor belongs to a typical implosion type. In coal rock tremors, such as roof shear rupture, masonry beam structure slip instability, dynamic burst of coal pillar, and mining-induced fault activation, the P-wave first motion is distributed in four quadrants in space, which is in line with the focal rupture mechanism of a typical double-couple source. They can be regarded as shear-type (Gibowicz et al., 1990; Du et al., 2020a). Mining-induced tremors of this type whose failure process is intense with more vibratory energy released and the highest burst risk.

Since the arrangement of each microseismic station is affected by the fluctuation of the coal seam and does not have a planar position relationship with the tremor events, the confirmed P-wave first motion of mining-induced tremors is not only simply upward or downward, but also should be determined according to the spatial position relationship between specific tremor events and corresponding stations.

The P-wave first motion of previous burst events is displayed in **Table 4**. It can be seen that: *1*) the P-wave first motions of the same station in different burst events are not completely the same, indicating that the microseismic waveform can fully reflect the characteristics of mine geological structure, mining environment, and overburden structure. *2*) The P-wave first motions of different stations in the same burst event are different, including compression P-waves and expansion P-waves with roughly the same proportions. Each burst event distributes in four quadrants, which is consistent with the focal rupture mechanism of a typical double-couple source. However, some channels were too far away from the source to receive an effective waveform. Moreover, as some stations were affected by mining activities with much background noise, the accurate direction of the P-wave first motion cannot be recognized.

Ratio of Es/Ep of Mining-Induced Tremors

The limitation of the P-wave first arrival method is that the closer the source is to the fault discontinuous surface, the weaker the P-wave is and the more difficult it is to identify the direction of the first motion. In the process of focal mechanism research in the Ruhr mining area, Germany, researchers found that the energy ratio of shear wave (S-wave) to compression wave (P-wave) is an important indicator to reveal the rupture mechanism of surrounding rocks. In recent years, with abundant on-site failure cases, many studies have been conducted on the discrimination criterion for determining the mechanism of coal rock mass fracture based on the distribution of the ratio of Es/Ep (Cai et al., 1998; Hudyma and Potvin, 2010; Kwiatek and Ben-Zion, 2013; Li et al., 2014). Subsequent studies demonstrate that the S-wave radiation energy is much larger than the P-wave radiation energy in earthquakes induced by fault slip (Boatwright and Fletcher, 1984), and that this kind of earthquake is dominated by shear

TABLE 4 | P-wave first motion of previous burst events.

Station number / Burst event	1#	2#	3#	4#	5#	6#	7#	8#	9#	10#	11#	12#	13#	14#	15#	16#	17#
2018.07.06	–	–	+	+	●	+	–	–	–	+	○	–	●	–	+	–	–
2019.03.07	–	+	+	●	+	+	–	–	–	+	+	–	–	–	+	–	–
2019.05.09	+	+	+	○	–	+	–	+	+	+	○	+	○	–	+	+	+
2019.06.29	–	+	–	–	+	+	+	+	+	+	+	+	–	–	–	+	+
2019.09.12	+	+	+	+	+	+	+	+	+	+	–	–	–	+	+	+	–
2019.10.06	+	+	+	+	+	+	–	–	+	+	+	+	+	–	–	+	–
2019.11.25	–	+	+	○	+	+	–	+	+	–	○	+	+	–	–	–	+
2019.12.24	+	+	–	+	+	+	+	–	–	–	–	–	+	●	+	+	+
2020.01.08	+	–	–	+	–	+	+	–	–	–	–	○	+	–	–	○	+
2020.05.24	–	+	+	+	●	–	+	–	–	+	+	+	+	+	+	–	+

+, compressed P-wave; –, expansion P-wave; ○, no valid waveform is received; ●, P-wave first motion cannot be identified due to too much background noise.

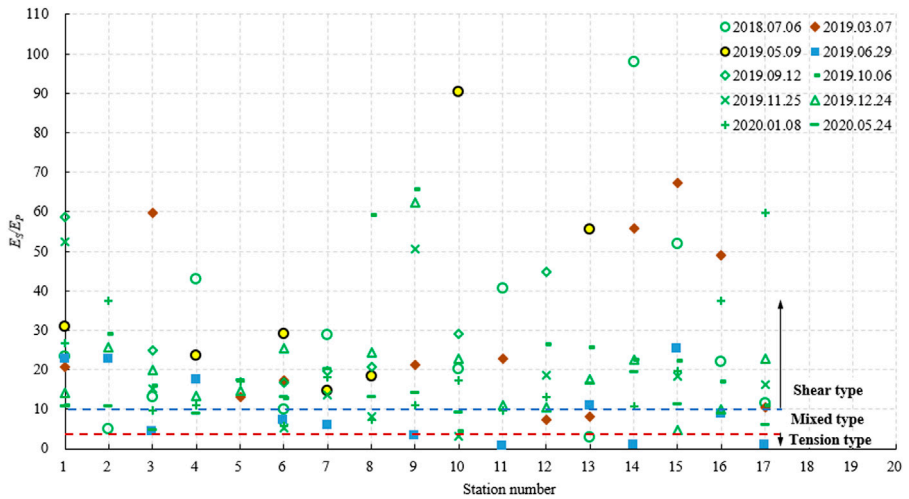

FIGURE 11 | *Es/Ep* in each channel of previous burst events.

failure. The P-wave and S-wave energies detected by the MS system can be calculated by using **the**following equation (Mendecki, 1997):

$$\begin{aligned} E_p &= \frac{8}{5}\pi\rho v_p R^2 \int_0^{t_s} \dot{u}_{corr}^2(t)dt, \\ E_s &= \frac{8}{5}\pi\rho v_s R^2 \int_0^{t_s} \dot{u}_{corr}^2(t)dt, \\ E_p &= \frac{8}{5}\pi\rho v_p R^2 \int_0^{t_s} \dot{u}_{corr}^2(t)dt, \\ E_s &= \frac{8}{5}\pi\rho v_s R^2 \int_0^{t_s} \dot{u}_{corr}^2(t)dt, \end{aligned} \tag{2}$$

where E_p and E_s are the radiation energies of P-wave and S-wave, respectively; ρ is the rock density; v_p and v_s are the wave velocities of P-wave and S-wave, respectively; R is the distance between the station and the source; t_s is the duration of the source; and $\dot{u}_{corr}^2$ is the square of the far-field corrected radiation direction of the velocity pulse. In this study, the burst mining-induced tremors whose *Es/Ep* is larger than 10 in each channel are regarded as shear rupture; those whose *Es/Ep* is smaller than three are regarded as tension rupture and those whose *Es/Ep* ranges from three to 10 are regarded as mixed rupture (Wang et al., 2019; Du et al., 2020b; Wang et al., 2021).

Attenuation correction in the frequency domain was carried out for the body wave frequency spectrum detected in each channel of all burst events, and frequency integration was carried out for the velocity power spectrum to estimate the radiation energy fluxes of P-wave and S-wave and to further identify the rupture type. According to the results given in **Figure 11**, the basic rules are as follows: *1*) The distance and path between each station and the source are different, and the difference in attenuation of seismic wave results in different P-wave and S-wave energies at each station. The closer it is to the source, the shorter the vibration time, and the less the attenuation, therefore the higher the energy monitored by the

station; otherwise, the farther away from the source, the lower the energy monitored. The energy of the same source detected in different stations can differ by up to two orders of magnitude. *2*) All the E_p in each channel of signal waveform of previous burst accidents in Mengcun coal mine are smaller than E_s with the value of E_p / E_s ranging from 3.01 to 65.69. The burst tremor waveform channels whose *Es/Ep* is smaller than three account for 1.28%, those with *Es/Ep* that lie in the range of 3–10 account for 19.23%, and those whose *Es/Ep* is greater than 10 account for 79.49%. Such a result demonstrates that the mining-induced tremors in the main entry area are mainly shear type and mixed type, which accords with the focal mechanism of CBTMIFS.

Based on the aforementioned analysis, the cause of the frequent destructive mining-induced tremors in the main entry area can be concluded as follows: The mining stress affects the F29 fault in a closed state, releasing the clamping normal stress of the long-term geological tectonic movement on the normal-line direction of the fault surface, which results in a rapid rise of shear stress of the fault surface and the "activation" of the previously stable fault. The slip dislocation of the fault surface in the main entry area gives rise to shear failure, which leads to slip instability of the fault and dynamic burst failure to the entries.

At the same time, it should be noted that different from the common burst failure induced by pushing mining across faults on the working face, this kind of burst failure mainly occurs in the main entries far from the working face, rather than on the working face. Research shows that more than 91% of coal burst events occur in the two lanes ahead of the working face, which seems to be in contradiction with the research object of this study. The coal rock mass in the fault area is weakened by pre-pressure relief measures in advances such as large diameter coal drilling, coal blasting, and roof pre-splitting blasting during entry excavation and mining, which undermines the F29 fault structure to a certain extent. The release of massive accumulated elastic energy lowers the degree of stress concentration and energy accumulation in the process of mining on the working face when crossing fault. However, the main entries, as the development roadway that needs to be used for a long time, lack the condition of frequent construction pressure relief engineering to ensure sufficient entry support effect. Consequently, coal stress becomes highly concentrated at the junction of the main entries and the fault. Under the influence of mining stress and tectonic stress, the hanging wall and the heading wall of the fault slip relative to each other, releasing massive strain energy instantly.

In addition, different from the common tension-type mining-induced tremors caused by roof stretching and implosion-type tremors by coal pillar compression, the frequency of fault slip is lower than that of the former two, but the vibration energy released is more and the failure is greater due to the volume of rock mass reaching the limit state at the source is larger (the potential source radius is larger).

CONCLUSION

Through the establishment of numerical simulation and the analysis of the microseismic signal characteristics of the burst events, the dynamic evolution characteristics of normal stress, and shear stress on the fault surface of the working face during the mining process, the influence of different horizontal stresses on the evolution of the stress field and energy field of fault slip, and the P-wave first motion and focal mechanism revealed by the ratio of E_S/E_P based on the spectrum characteristics of shake displacement are investigated, respectively. The main conclusions are as follows:

1. The geological structure leads to significant abnormal horizontal stress in the accident area, and the stratum deposition is obviously controlled by the tectonic movement of faults and folds, leading to stratum inversion, and deletion of overburden. The faults under high-stress conditions provide a favorable external environment for frequent coal burst accidents.
2. Different from common coal burst accidents in the working face, coal burst accidents induced by mining fault slip under high-stress conditions have significant shear seismic failure characteristics, i.e., with more complex failure type, larger failure scope, and higher failure degree. The failure characteristics in common are as follows: the hanging wall effect is obvious; the more energy released during a coal burst, the more destructive it will be to the entry; the heterogeneous stress evolution of the fault surface leads to the characteristics of multiple and repeated bursts of the entry.
3. The normal stress and shear stress on the fault surface show a dynamic heterogeneous evolution due to mining unloading, and the normal stress gradually decreases with mining, while the shear stress increases gradually due to shear slip, and the change rate of shear stress is greater than that of normal stress. The value of normal stress experienced a "positive-negative-positive" change process with mining, indicating that the main stress field on the fault surface rotates due to mining disturbance. This can be regarded as the precursor of fault slip. Under different initial ground stress levels, the higher the horizontal stress is, the higher the normal stress and shear stress on the fault surface will be. Besides, the greater the strain energy accumulated before the fault slip and released now of the slip is, the higher the corresponding burst risk will be.
4. The microseismic signals of burst accidents feature "high energy and low frequency," and the value of the fractal dimension D is high, and the S-wave is relatively developed, which accords with the characteristics of the shake displacement spectrum of typical shear mining-induced tremors. The P-wave first motion of each channel is distributed in four quadrants, which conforms to the focal rupture mechanism of a typical double-couple source. According to the E_S/E_P ratio of burst waveform, the destructive mining-induced tremors are mainly shear and mixed types.

Therefore, it can be concluded that frequent destructive tremors in the main entry area are caused by the mining stress affecting the F29 fault in a closed state, releasing the clamping normal stress of the long-term geological tectonic movement in the normal-line direction of the fault surface. Resultantly, the shear stress of the fault surface rises rapidly, and the previously stable fault becomes activated. The slip dislocation of the fault surface in the main entry area gives rise to shear failure, which leads to slip instability of fault and dynamic burst failure of the entries. The research conclusions disclose the mechanism of CBTMIFS under high-stress conditions, which is of great significance to further enriching the cognition of the inducing mechanism of fault coal burst.

DATA AVAILABILITY STATEMENT

The original contributions presented in the study are included in the article/Supplementary Material, further inquiries can be directed to the corresponding authors.

AUTHOR CONTRIBUTIONS

JB contributed to conceptualization, methodology, software, data curation, validation, writing—original draft, and funding acquisition. LD contributed to data curation, writing—review and editing, and funding acquisition. JL contributed to supervision, writing—review and editing, and funding acquisition. KZ contributed to writing—review and editing and funding acquisition. JC contributed to writing—review and editing. JK contributed to funding acquisition and writing—review and editing.

FUNDING

The authors gratefully acknowledge the financial support for this work provided by the Postgraduate Research & Practice Innovation Program of Jiangsu Province (Grant No. KYCX21_2342) and National Natural Science Foundation of China (Grant Nos 51874292 and 52004004).

REFERENCES

Bai, Q., Konietzky, H., Ding, Z. W., Cai, W., and Zhang, C. (2021). A Displacement-dependent Moment Tensor Method for Simulating Fault-Slip Induced Seismicity. *Geomech. Geophys. Geo-energ. Geo-resour.* 7, 79. doi:10.1007/s40948-021-00269-y

Bieniawaki, Z. T. (1967). Mechanism of Brittle Fracture of Rock, Parts I, II, III. *Int. J. Rock Mech. Min. Sci. Geomechanics Abstr.* 4 (4), 395–430. doi:10.1016/0148-9062(67)90031-9

Blake, W., and Hedley, D. G. F. (2003). *Rockbursts: Case Studies from North American Hard-Rock Mines*. Littleton: Society for Mining, Metallurgy, and Exploration, Inc.

Boatwright, J., and Fletcher, J. B. (1984). The Partition of Radiated Energy between P and S Waves. *Bull. Seismol. Soc. Am.* 74, 361–376. doi:10.1785/bssa0740020361

Byerly, P. (1928). The Nature of the First Motion in the Chilean Earthquake of November 11, 1922. *Am. J. Sci.* s5-16, 232–236. doi:10.2475/ajs.s5-16.93.232

Cai, M., Kaiser, P. K., and Martin, C. D. (1998). A Tensile Model for the Interpretation of Microseismic Events Near Underground Openings. *Pure Appl. Geophys.* 153, 67–92. doi:10.1007/978-3-0348-8804-2_5

Cai, W., Dou, L. M., Zhang, M., Cao, W., Shi, J.-Q., and Feng, L. (2018). A Fuzzy Comprehensive Evaluation Methodology for Rock Burst Forecasting Using Microseismic Monitoring. *Tunn. Undergr. Space Technol.* 80, 232–245. doi:10.1016/j.tust.2018.06.029

Cai, W., Dou, L., Si, G., and Hu, Y. (2020). Fault-Induced Coal Burst Mechanism under Mining-Induced Static and Dynamic Stresses. *Engineering* 7 (5), 687–700. doi:10.1016/j.eng.2020.03.017

Cook, N. G. W. (1976). Seismicity Associated with Mining. *Eng. Geol.* 10 (2–4), 99–122. doi:10.1016/0013-7952(76)90015-6

Du, K., Li, X.-f., Yang, C.-z., Zhou, J., Chen, S.-j., and Manoj, K. (2020b). Experimental Investigations on Mechanical Performance of Rocks under Fatigue Loads and Biaxial Confinements. *J. Cent. South Univ.* 27 (10), 2985–2998. doi:10.1007/s11771-020-4523-7

Du, K., Li, X., Tao, M., and Wang, S. (2020a). Experimental Study on Acoustic Emission (AE) Characteristics and Crack Classification during Rock Fracture in Several Basic Lab Tests. *Int. J. Rock Mech. Min. Sci.* 133, 104411. doi:10.1016/j.ijrmms.2020.104411

Du, K., Li, X., Wang, S., Tao, M., Li, G., and Wang, S. (2021). Compression-Shear Failure Properties and Acoustic Emission (AE) Characteristics of Rocks in Variable Angle Shear and Direct Shear Tests. *Measurement* 183, 109814. doi:10.1016/j.measurement.2021.109814

Duan, K., Ji, Y., Xu, N., Wan, Z., and Wu, W. (2019). Excavation-Induced Fault Instability: Possible Causes and Implications for Seismicity. *Tunn. Undergr. Space Technol.* 92, 103041. doi:10.1016/j.tust.2019.103041

Fan, L. F., and Wong, L. N. Y. (2013). Stress Wave Transmission across a Filled Joint with Different Loading/Unloading Behavior. *Int. J. Rock Mech. Min. Sci.* 60, 227–234. doi:10.1016/j.ijrmms.2012.12.046

Gibowicz, S. J., Harjes, H. P., and Schafer, M. (1990). Source Parameters of Seismic Events at Heinrich Robert Mine, Ruhr Basin, Federal Republic of Germany: Evidence for Nondouble-Couple Events. *Bull. Seism. Soc. Am.* 80, 88–109. doi:10.1016/0040-1951(90)90194-D

Gibowicz, S. J., and Kijko, A. (1994). *An Introduction to Mining Seismology*. San Diego: Academic Press.

Hasegawa, H. S., Wetmiller, R. J., and Gendzwill, D. J. (1989). Induced Seismicity in Mines in Canada?An Overview. *Pageoph* 1989 (129), 423–453. doi:10.1007/BF00874518

Herrmann, R. B. (1975). A Student's Guide to the Use of P and S Wave Data for Focal Mechanism Determination. *Seismol. Res. Lett.* 46, 29–39. doi:10.1785/gssrl.46.4.29

Horner, R. B., and Hasegawa, H. S. (1978). The Seismotectonics of Southern Saskatchewan. *Can. J. Earth Sci.* 15 (15), 1341–1355. doi:10.1139/e78-139

Hudyma, M., and Potvin, Y. H. (2010). An Engineering Approach to Seismic Risk Management in Hardrock Mines. *Rock Mech. Rock Eng.* 43, 891–906. doi:10.1007/s00603-009-0070-0

Husen, S., Kissling, E., and von Deschwanden, A. (2013). Induced Seismicity during the Construction of the Gotthard Base Tunnel, Switzerland: Hypocenter Locations and Source Dimensions. *J. Seismol.* 17 (1), 63–81. doi:10.1007/s10950-011-9261-810.1007/s10950-012-9313-8

Kaiser, P. K., Diederichs, M. S., Martin, C. D., Sharp, J., and Steiner, W. (2000). *Underground Works in Hard Rock Tunnelling and Mining. Keynote Lecture in Proceedings of GeoEng2000*, Vol. 1. Lancaster: Technomic Publishing Co., 841–926.

Kwiatek, G., and Ben-Zion, Y. (2013). Assessment ofPandSwave Energy Radiated from Very Small Shear-Tensile Seismic Events in a Deep South African Mine. *J. Geophys. Res. Solid Earth* 118, 3630–3641. doi:10.1002/jgrb.50274

Li, J., Ma, G., and Zhao, J. (2011). Analysis of Stochastic Seismic Wave Interaction with a Slippery Rock Fault. *Rock Mech. Rock Eng.* 44, 85–92. doi:10.1007/s00603-010-0109-2

Li, J., Wu, S. C., Gao, Y. T., Xie, Y., and Ji, M. (2014). Review of Slope Micro-seismic Monitoring in Open-Pit Mine. *Chin. J. Rock Mech. Eng. (in Chinese)* 33 (S2), 3998–4013. doi:10.13722/j.cnki.jrme.2014.s2.077

Marone, C. (1998). The Effect of Loading Rate on Static Friction and the Rate of Fault Healing during the Earthquake Cycle. *Nature* 391, 69–72. doi:10.1038/34157

McGarr, A. (1984). in *Some Applications of Seismic Source Mechanism Studies to Assessing Underground Hazard. Rockbursts and Seismicity in Mines*. Editors N. C. Gay and E. H. Wainwright (Johannesburg: Balkema), 1984, 199–208.

McGarr, A., Simpson, D., and Seeber, L. (2002). 40 Case Histories of Induced and Triggered Seismicity. *International Handbook of Earthquake and Engineering Seismology* 81A, 647–661. doi:10.1016/S0074-6142(02)80243-1

Mendecki, A. J. (1997). *Seismic Monitoring in Mines*. London: Chapman & Hall.

Morrow, C. A., and Byerlee, J. D. (1989). Experimental Studies of Compaction and Dilatancy during Frictional Sliding on Faults Containing Gouge. *Journal of Structural Geology* 11, 815–825. doi:10.1016/0191-8141(89)90100-4

Ortlepp, W. D., and Stacey, T. R. (1992). Rockburst Mechanisms in Tunnels and Shafts. *Tunnelling and Underground Space Technology* 30 (6), 59–65. doi:10.1016/0148-9062(93)91705-n

Pan, Y. S. (1999). *Study on Rock Burst Initiation and Failure Propagation [dissertation]Chinese*. Beijing: Tsinghua University.

Segall, P., and Rice, J. R. (1995). Dilatancy, Compaction, and Slip Instability of a Fluid-Infiltrated Fault. *J. Geophys. Res.* 100, 22155–22171. doi:10.1029/95JB02403

Suppe, J. (1983). Geometry and Kinematics of Fault-Bend Folding. *American Journal of Science* 283 (7), 684–721. doi:10.2475/ajs.283.7.684

Wang, S., Li, X., Yao, J., Gong, F., Li, X., Du, K., et al. (2019). Experimental Investigation of Rock Breakage by a Conical Pick and its Application to Non-explosive Mechanized Mining in Deep Hard Rock. *International Journal of Rock Mechanics and Mining Sciences* 122, 104063. doi:10.1016/j.ijrmms.2019.104063

Wang, S., Sun, L., Li, X., Wang, S., Du, K., Li, X., et al. (2021). Experimental Investigation of Cuttability Improvement for Hard Rock Fragmentation Using Conical Cutter. *Int. J. Geomech.* 21 (2), 06020039. doi:10.1061/(ASCE)GM.1943-5622.0001899

Wu, W., Zhao, Z., and Duan, K. (2017). Unloading-Induced Instability of a Simulated Granular Fault and Implications for Excavation-Induced Seismicity. *Tunnelling and Underground Space Technology* 63, 154–161. doi:10.1016/j.tust.2017.01.002

Yin, Z.-q., Li, X.-b., Jin, J.-f., He, X.-q., and Du, K. (2012). Failure Characteristics of High Stress Rock Induced by Impact Disturbance under Confining Pressure Unloading. *Transactions of Nonferrous Metals Society of China* 22 (1), 175–184. doi:10.1016/S1003-6326(11)61158-8

Yin, Z., Chen, W., Hao, H., Chang, J., Zhao, G., Chen, Z., et al. (2019). Dynamic Compressive Test of Gas-Containing Coal Using a Modified Split Hopkinson Pressure Bar System. *Rock Mech Rock Eng* 53 (1), 815–829. doi:10.1007/s00603-019-01955-w

Yin, Z. Q., Ma, H. F., Ma, H. F., Hu, Z. X., and Zou, Y. (2014). Effect of Static - Dynamic Coupling Loading on Fracture Toughness and Failure Characteristics in Marble. *Jestr* 7 (2), 169–174. doi:10.25103/jestr.072.25

Zhang, C., Canbulat, I., Hebblewhite, B., and Ward, C. R. (20172017). Assessing Coal Burst Phenomena in Mining and Insights into Directions for Future Research. *International Journal of Coal Geology* 179, 28–44. doi:10.1016/j.coal.2017.05.011

Zhao, Z., and Song, E.-x. (2015). Particle Mechanics Modeling of Creep Behavior of Rockfill Materials under Dry and Wet Conditions. *Computers and Geotechnics* 68, 137–146. doi:10.1016/j.compgeo.2015.04.008

Conflict of Interest: The authors declare that the research was conducted in the absence of any commercial or financial relationships that could be construed as a potential conflict of interest.

Publisher's Note: All claims expressed in this article are solely those of the authors and do not necessarily represent those of their affiliated organizations, or those of the publisher, the editors, and the reviewers. Any product that may be evaluated in this article, or claim that may be made by its manufacturer, is not guaranteed or endorsed by the publisher.